processes

MDPI

Article

Experimental and Numerical Simulation Study of Pressure Pulsations during Hose Pump Operation

Wendong Wang, Lixin Zhang *, Xiao Ma, Zhizheng Hu and Yongchun Yan

College of Mechanical and Electrical Engineering, Shihezi University, Shihezi 832003, China; wangwendong@stu.shzu.edu.cn (W.W.); maxiao@stu.shzu.edu.cn (X.M.); huzhizheng@stu.shzu.edu.cn (Z.H.); yanyongchun@stu.shzu.edu.cn (Y.Y.)

* Correspondence: Zhlx2001329@163.com

Abstract: An adventitious flow field has a great impact on the operational reliability of pumps; therefore, it is important to study pump flow characteristics to reduce the noise, vibration, and cavitation performance of pumps. To study the pressure fluctuation characteristics of the hose pump, a three-dimensional two-way fluid structure coupling model of the hose pump was established. The transient structural module, fluid flow (fluent) module, and system coupling module of ANSYS Workbench 19.0 were used to simulate the unsteady multiple working conditions of the hose pump. The accuracy and reliability of the calculation results from the fluid solid coupling simulation were verified via experimentation. The results show that the roller pass frequency is the main frequency of the pressure fluctuation at the outlet of the hose pump. When the plane of the deformation recovery area is small, the pressure pulsation amplitude is large, and the outlet pressure and speed are large. Due to the irregular backflow of the fluid, stall zones of different sizes form, the outlet pressure is closer to a sinusoid when there is no pressure. The higher the rotating speed is, the faster the pressure roller leaving the hose, the higher the pressure pulsation, and the larger the stall zone. Therefore, the best way to reduce the pressure pulsation in the pump is to optimize the geometry of the pressure roller and change the outlet angle of the hose.

Keywords: two-way fluid-structure coupling; experimental; frequency analysis; numerical simulation; pressure fluctuation

Citation: Wang, W.; Zhang, L.; Ma, X.; Hu, Z.; Yan, Y. Experimental and Numerical Simulation Study of Pressure Pulsations during Hose Pump Operation. *Processes* **2021**, *9*, 1231. https://doi.org/10.3390/pr9071231

Academic Editor: Gabriella Bognár

Received: 10 June 2021
Accepted: 2 July 2021
Published: 16 July 2021

1. Introduction

Hose pumps are widely used in wastewater and dirt treatment, the chemical industry, the food industry, brewing, the sugar manufacturing industry, the paper and ceramic industry, the construction industry, and the mining industry [1]. A hose pump is a kind of rotor pump [2]. It is composed of a pump body, hose and rotor. The squeezed pump pipe in the pump head forms a pillow-like shape between the two rollers, which is usually called a "pillow" [3]. The existence of the pillow causes the volume of each revolution of the pump head to be exact, and the flow rate is relatively accurate [4]. However, when one end of the pillow is about to flow out of the pump head, because the previous roller has lost pressure on the pump pipe [5], the recovery deformation of the pump pipe makes a part of the liquid flow back to the recovery deformation area of the pump pipe, so the liquid in the pump pipe is not at a constant velocity flow [6,7], and it changes periodically. This kind of flow causes the pump pipe to produce periodic beating, which is called the "pulsation" phenomenon [8]. Hose pumps are named because their working principle is similar to that of the digestive tract, which transports gas, solids, and liquids in a peristaltic way. The designer and user of the hose pump attach great importance to its ability to deliver a strong abrasive medium. It has no valve and no seal. The only component contacting the medium is the inner cavity of the rubber hose [9,10]. The rotor of the compressed hose is completely independent of the medium [11]. The hose pump not only takes into account the delivery of high viscosity and corrosive liquid [12,13]. Due to the pulsation phenomenon of the

hose pump, it has a great influence on the pump body and accuracy. To better study the unsteady flow and pulsation of pump fluid, this paper intends to combine both numerical simulation and experiments.

To accurately describe the model behaviour of the hose pump, it is necessary to combine the fluid model with a solid model because fluid flow is caused by pipe extrusion. There is a strong coupling relationship between pipe deformation and fluid flow, so fluid-structure interaction (FSI) analysis is needed. Then, the modelling of FSI is mainly focused on the pulsating flow caused by the motion domain. An important part of solving FSI problems is the mesh mobility technique (MMT), which is used to adapt computational grids in the mobile fluid domain. The ideal MMT can be easily computed; it can deal with large mesh motion without reversing the mesh elements and can maintain FSI simulation for a long time without irreversibly distorting the mesh. However, due to the large deformation of the hose, the convergence of fluid and structure is difficult, and the amount of computation is extensive.

Alexander Shamanskiy [14] compared several MMTSs based on solutions of elliptical partial differential equations, including harmonic extension, double harmonic extension, and techniques based on linear elastic equations. In addition, a special MMT was proposed, which uses the idea of a continuous method to solve nonlinear elastic equations effectively. Yakhlef Othman [15] proposed an implicit scheme to solve the dynamic fluid structure interaction problem through a step-by-step program. For fluid equations (Stokes or Navier–Stokes), the virtual domain method with penalty is used. The penalty function is used to obtain the velocity equality of the fluid and structure at the interface. The fluid solution in the domain is used to calculate the surface force at the fluid structure interface. Akbay Muzaffer [16] proposed a boundary pressure projection method, which can reduce the incompatibility while maintaining the decomposed Dirichlet Neumann structure without modifying the fluid or solid solver. Zhang Ning et al. [17] proposed a new immersed boundary method for compressible fluid structure interaction simulation. The strategy consists of three parts: fluid solver, structure solver, and fluid solid boundarytreatment. The fluid solver is implemented by the second-order finite volume scheme, while the structure is implemented by the implicit finite element solver. For the boundary treatment, the multilevel marking algorithm is used to determine the direction from the inside to the outside of the structure.

Xiaoming Zhou [18] established a generalized parameter model of a typical roller pump system and derived the analytical expression of the motion boundary. Based on the model and formula, the dynamic geometry and grid of the flow field can be updated automatically according to the roll position changing with time. The described method successfully simulates the pulse flow generated by the pump. Elabbasi [19] used the 3D FSI of COMSOL multiphysics to study the performance of a 180 degree rotating peristaltic pump with two metal rollers. The fluid part and the structure part are unified in this model. The structural part and the fluid part are described by the Mooney Rivlin hyperelastic material model and laminar flow model, respectively. The flow parameters of the peristaltic pump were accurately designed, and theoretical calculations and an experimental verification were carried out. Daochen Wang [20] analysed the factors influencing the flow rate of peristaltic pumps and compared the experimental and theoretical values of the flow rate of peristaltic pumps. The experimental value was approximately 66% of the theoretical value. On the basis of Wang Daochen, Junping Liu [21] and others considered the influence of the volume occupied by the roller on the flow rate and optimized the flow rate calculation formula.

From the above literature, most of the research on the pulsation of hose pumps is based on a comparison between theoretical calculations and experiments and simply proposes that the existence of pulsation affects the flow rate. Most of the theoretical research on fluid structure coupling is not applied to the specific model, but the calculation model is optimized in a different way. Little research has been conducted on the pulsation characteristics of hose pumps.

Therefore, it is particularly important to analyse the unsteady flow characteristics of the hose pump to improve the operational reliability of the pump. The purpose of this study is to analyse and predict the unsteady pressure fluctuation distribution area of a hose pump. First, through experiments and numerical measurements, the time domain and frequency domain of pressure fluctuations are analysed. The results can be used as a theoretical reference for the optimization of hose pumps.

2. Simplified Model and Numerical Calculation Method of the Pump

2.1. Geometric Model and Finite Element Mesh

In the working process of the hose pump, three rollers extrude an elastic hose. The fluid is pushed forward through the hose during the compression and relaxation stages. To better study the fluid flow and pulsation characteristics of the hose pump, a three-dimensional two-way fluid-structure coupling model of the hose pump was established. The transient structural module, fluid flow (fluent) module, and system coupling module were used in ANSYS Workbench 19.0. The FSI model of the hose pump consists of three rollers, a U-shaped hose, and a U-shaped base. The U-shaped base device restricts pipe movement in the extrusion stage. The model parameters of the hose pump are shown in Table 1. Finally the computational domain containing seven parts is established for numerical simulation, namely the inlet and outlet, the roller, the base, the tube and base contact surface, the roller and tube contact surface and the fluid solid interface, as shown in Figure 1.

Table 1. Material parameters of the hose.

Rotor Speed	Number of Rollers	Diameter of Roller	Diameter of Outer Circler	Hose Inlet Diameter	Hose Outer Diameter
r/min	Pcs	mm	mm	mm	mm
30–60	3	69	260	25	25

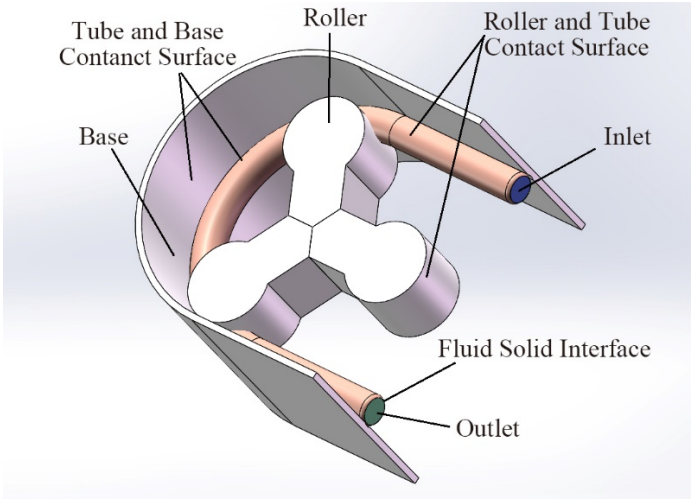

Figure 1. Three-dimensional finite element schematic diagram.

Because the three rollers of the hose pump allow the initial simulation model of the hose pump to be penetrated, this study adopts the method of assembling the initial model first and then rotating it, as shown in Figure 2.

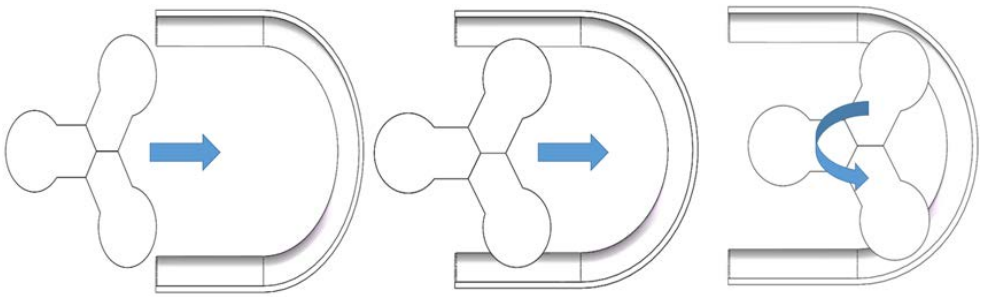

Figure 2. Assembly process diagram.

2.2. Grid Generation

During the working process of the hose pump, the liquid flows by squeezing the hose with the roller, resulting in large deformation of the hose and large deformation of the fluid domain, so the requirement of the grid is very high. ANSYS-ICEM 19.0 is used to establish a high-quality hexahedral structure grid and tetrahedral grid. To accelerate the calculation speed and maintain the iteration accuracy, a tetrahedral grid is used for the fluid, as shown in Figure 3, and a hexahedral grid is used for the hose roller base, as shown in Figure 4. In this study, an enhanced wall treatment is used to solve the complex flow structure near the solid wall.

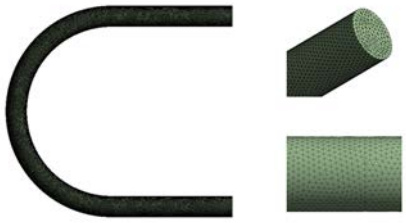

Figure 3. Fluid grid structure.

(**A**) Roller (**B**) Base

(**C**) Hose

Figure 4. Solid grid structure.

2.3. Model Establishment

In transient analysis, due to the continuous extrusion of the hose by the roller, the hose has a large deformation, and there is face-to-face contact between the hose and the roller and between the hose and the outer base. Therefore, the face-to-face contact element is

used to establish the contact relationship, and the augmented Lagrange function is selected for the contact algorithm.

In the transient analysis, the finite deformation of the pipe in the extrusion process makes the turbulent structure rise, the range of Reynolds number on the suction side and pressure side is 6000–15,000. To simulate the actual flow of fluid in the rubber hose of the hose pump, it is necessary to establish a turbulence model, and the fluid is described in an arbitrary Lagrange Eulerian (ALE) framework. The ALE derivative induced by a deformation of the fluid domain, $\varphi : \Omega_0^f \times \mathrm{I} \to R^3$ for a scalar function $\varphi : \Omega_0^f \times \mathrm{I} \to R^3$ is defined as [22–25]:

$$\frac{D^{\varphi} f}{D\mathrm{t}} := \frac{\partial f}{\partial t} + \frac{\partial \phi}{\partial t} \cdot \nabla f \tag{1}$$

The deformed fluid domain is defined as $\forall t \in \mathrm{I}$ as $\Omega_t^f := \phi(\Omega_0^f, \mathrm{t})$. The fluid motion was described by the $RNG_{\kappa-\varepsilon}ALE$ turbulence model in an ALE framework [26,27]:

$$\rho^f \frac{D^f U^f}{D\mathrm{t}} + \rho^f (U^f - \omega)\nabla U^f = \nabla P^f + (\mu^f + \mu_t)\Delta U^f - \frac{2}{3}\nabla \mathrm{K} \tag{2}$$

$$\nabla U^f = 0 \tag{3}$$

$$\rho^f \frac{D^f k}{D\mathrm{t}} + \rho^f (U^f - \omega)\nabla U^f \cdot \nabla \mathrm{K} = \nabla P^f + (\mu^f + \frac{\mu_t}{\sigma_k})\Delta k - \rho^f \in + P_K \tag{4}$$

$$\rho^f \frac{D^{\Phi} \in}{D\mathrm{t}} + \rho^f (U^f - \omega)\nabla \in = (\mu^f + \frac{\mu_t}{\sigma_{\in}})\Delta \in - C_{2\in}\rho^f \frac{\in^2}{k} \in + \frac{\in}{k} C_{1\in} P_K - R_{\in} \tag{5}$$

where U^f is the mean velocity field, P^f is the mean pressure, k is the turbulent kinetic energy, $\in$ is the turbulent dissipation energy, ρ^f is the fluid density, μ^f is the fluid dynamic viscosity,P_K is the rate of production of turbulence,$R_{\in}$ is the rate of dissipation, and μ_t is the turbulent dynamic viscosity. The coefficients σ_k, $\sigma_{\in}$, $C_{1\in}$ and $C_{2\in}$ are closure coefficients.

The pipe displacement was determined by a neo-Hookean hyperelastic model in a Lagrangian framework:

$$\rho^s \frac{d^2\eta^2}{dt^2} + \rho^s \alpha \frac{d\eta^2}{dt} - \nabla \mathrm{T}^s - \beta \frac{d}{dt}\nabla \mathrm{T}^s = 0 \tag{6}$$

where ρ^s is the displacement field, ρ^s is the pipe density, T^s is the stress tensor,α is the mass damping coefficient, and β is the stiffness damping coefficient.

The interaction between the pipe and the roller is frictionless without considering the dissipation factor. For the fluid part, the standard slip-free condition is adopted, and the wall roughness of all flow fields is smooth. The working fluid is water at 25 °C, and the density $\rho^f = 10^3$ kg/m^3. The volume of the hose is almost constant when it is extruded, so it is classified as a hyperelastic material [28–32], as shown in Table 2. Assuming that there is no friction between the hose and the base, the self-contact of the hose is excluded.

Table 2. Material parameters of the pipe.

ρ^s	E	V	C_{10}	D_1	α	β
kg/m^3	MPa		MPa	MPa^{-1}	s^{-1}	s
2700	52	0.49	127	48	0.4	0.1

The ρ^s parameter is the density, the E parameter is the Young's modulus, the V parameter is the Poisson ratio, the C_{10} parameter weights the deformation of the body, the D_1 parameter weights the effect of compressibility along the motion, the α parameter is the mass damping coefficient and β is the stiffness damping coefficient.

2.4. Distributions of Monitoring Points and Areas

To analyse the flow field and pressure fluctuation characteristics inside the hose, seven monitoring points are set in the recovery deformation area of the hose, as shown in Figure 5. They are distributed on the suction and pressure sides of the roller. As the remaining gap between the hose and the closure increases gradually when the roller leaves the hose, the monitoring point of the pressure measurement is located in the middle of the middle plane. The monitoring surface is the radial section of the whole flow channel.

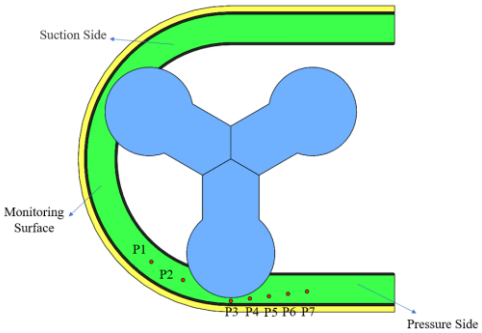

Figure 5. Distribution of monitoring points and monitoring surfaces.

3. Experimental Set Up

Test Rig Description

Experimental tests were carried out in an open test rig system, and the test rig schematics are shown in Figure 6. To adjust the outlet pressure, a valve was installed at the end of the outlet pipeline to adjust the pressure by adjusting the opening and closing degree of the valve. The inner diameter and outer diameter of the inlet pipe were 25 mm and 32 mm, respectively, and the inner diameter and outer diameter of the outlet pipe were 25 mm and 32 mm, respectively. A high-precision pulsating pressure sensor (0–5 V) is installed on the pipeline near the outlet to measure the pulsating pressure in the pipeline, and an electromagnetic flowmeter is installed on the pipeline to measure the flow change under different pulsating pressures. The data of the whole test bed are collected in real time by a data acquisition card.

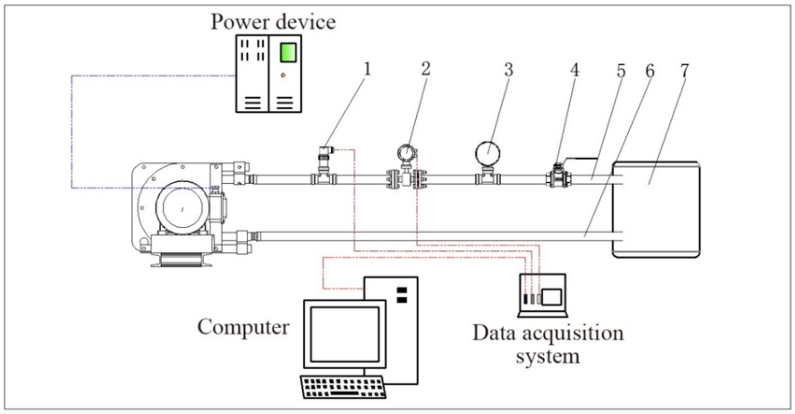

Figure 6. Scheme of the test rig. 1. Pulsating pressure sensor; 2. electromagnetic flowmeter; 3. pressure gauge; 4. valve; 5. outlet pipe; 6. inlet pipe; 7. water tank.

The test system and tested pump are shown in Figure 7. The pump was started by observing all standard start-up procedures and run until a suitable operating condition was reached. By adjusting the outlet valve of the pump to change the pipeline resistance of the experimental system, the performance parameters of the pump under different working conditions were obtained. Taking the speed and outlet pressure as the boundary conditions,

consistency between the numerical simulation and experimental results was effectively ensured. The 2S data were selected to calculate the pulsating pressure in the pipeline when the outlet pressure is different at different speeds, and the pressure pulsating characteristics are evaluated from the measured variables.

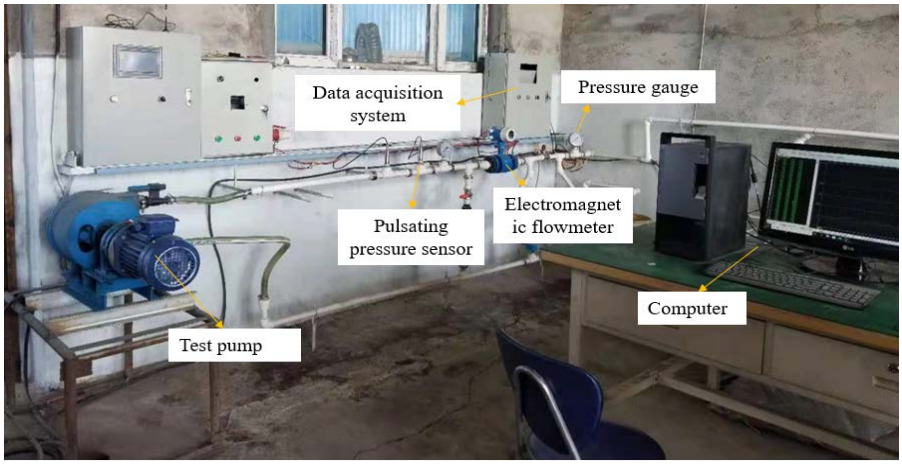

Figure 7. Test system of the test pump.

4. Results and Analysis

In the actual assembly process of the hose pump, the actual roller extrudes the hose completely, but the simulation must follow the conservation of energy to achieve good convergence, and there is a gap of 2.5 mm on the inner wall of the hose. Therefore, in the pressure loading process, the leakage increases gradually with increasing maximum pressure, but the flow tends to be stable at high speed. Flow leakage can have certain influences on the change in the flow field in the hose. At different speeds, because the roller squeezes the hose to induce different flow speeds, the rotational speeds of the hose pump are 35 r/min, 55 r/min, and 65 r/min. According to the calculation of the experimental results, when working at three speeds, the flow velocities at the suction side of the fluid are approximately 0.24 m/s, 0.35 m/s and 0.6 m/s, respectively. In the simulation, the inlet speeds are set as 0.24 m/s, 0.35 m/s, and 0.6 m/s. The outlet pressure is 0 MPa and 0.1 MPa. In this way, we can see the fluid flow in the hose and the pressure change very intuitively, as shown in Figure 8, and the error of the experiment and simulation is controlled within 5%, which verifies the correctness of the model. This method, combined with experiments, can better study the pulsation of hose pumps.

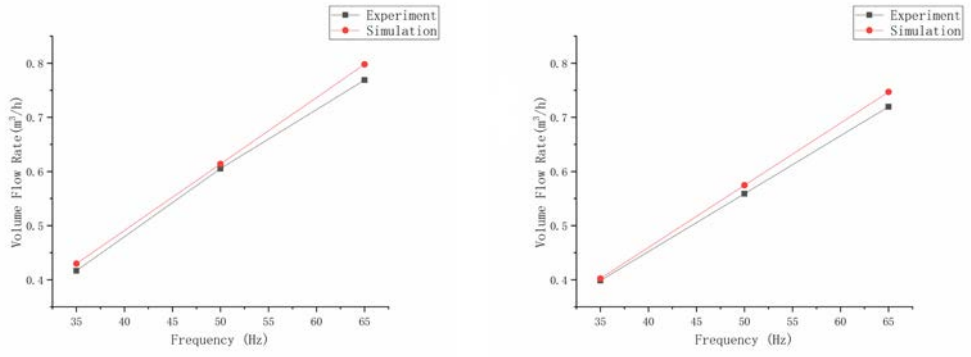

(**a**) The outlet pressure is 0 MPa (**b**) The outlet pressure is 0.1 MPa

Figure 8. Flow curve of experimental and simulation results.

4.1. Static Pressure Distribution

Figures 9 and 10 show the static pressure distribution at different speeds when the roller leaves the hose at 0 MPa and 0.1 MPa outlet pressure. Here, the moment $t = t_0$ represents that the hose pump to reach stable operation, $t_0 = 1$ s, and Δt is the time step of the CFD approach, $\Delta t = 0.002$ s. When the outlet pressure is 0 MPa, the static pressure changes at each speed are almost the same. As shown in Figure 11, when the roller turns to 270 degrees, at $t = t_0 + 235\Delta t$ moment, the pressure on the suction side is less than that on the pressure side. With the roller continuing its motion to $t = t_0 + 325\Delta t$, the pressure on the suction side increases and the pressure on the pressure side decreases. Then, because the liquid squeezed by the latter roller flows forward, the former roller gradually leaves the hose. At $t = t_0 + 325\Delta t$ moment, the roller just leaves the hose, the static pressure distribution on the pressure side gradually becomes uniform. When the outlet pressure is 0.1 MPa, the change in static pressure in the hose is almost the same as that when the outlet pressure is 0 MPa. Under the same pressure, with the increase in rotating speed, the speed of the pressure roller leaving the hose increases, the static pressure in the hose shows circumferential non-uniformity, and the axial non-uniformity of static pressure becomes more obvious, The range of fluctuating pressure is (−22.42–1733 pa). At the same speed, with increasing outlet pressure, the static pressure in the hose changes obviously, and the range of fluctuating pressure is (−30.16–102,000 pa).

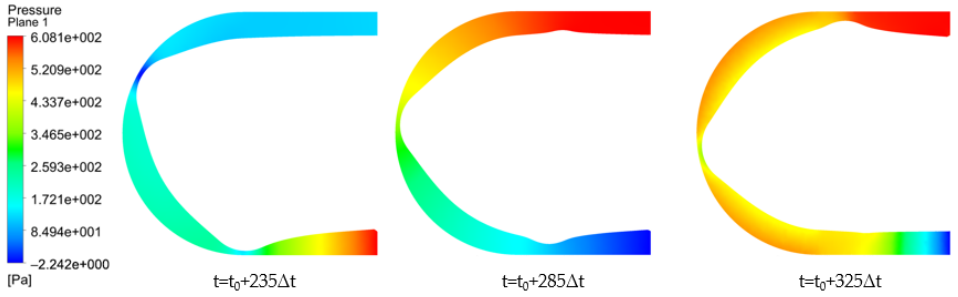

(**a**) 35 r/min

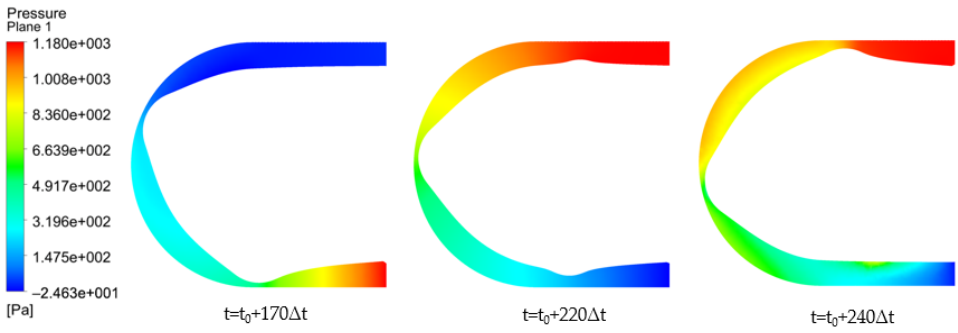

(b) 50 r/min

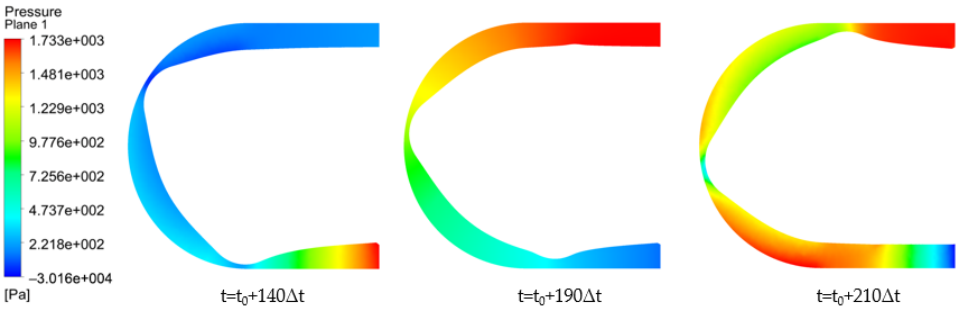

(**c**) 65 r/min

Figure 9. Static pressure distribution of the 0 MPa outlet pressure at different speeds.

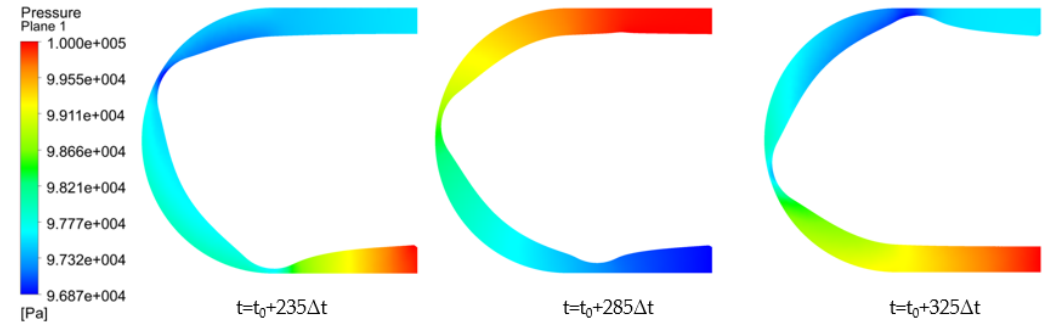

(**a**) 35 r/min

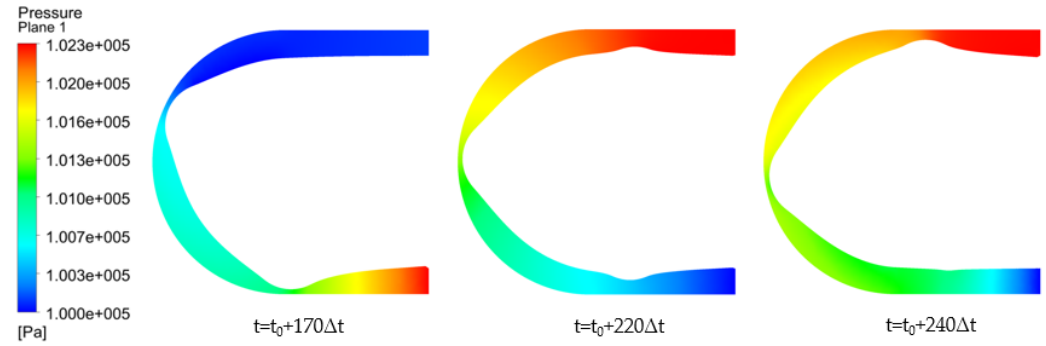

(**b**) 50 r/min

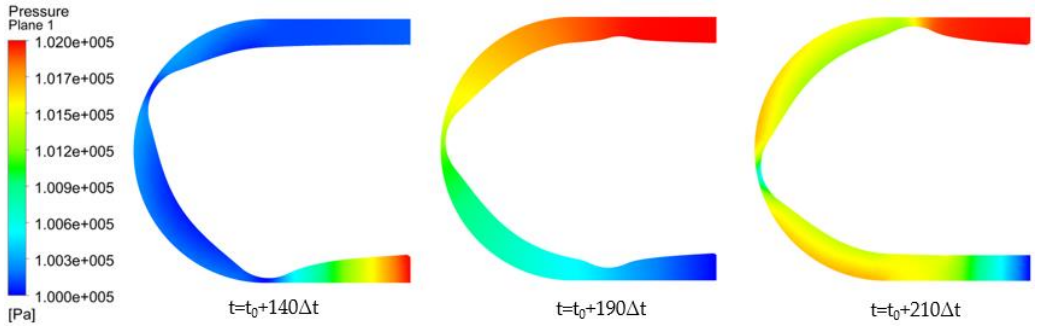

(**c**) 65 r/min

Figure 10. Static pressure distribution of the 0.1 MPa outlet pressure at different speeds.

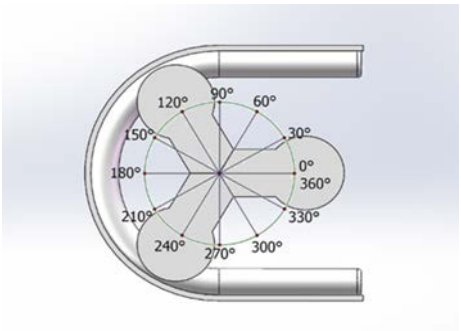

Figure 11. Rotation angle of roller.

4.2. Velocity Streamline Distribution

When the outlet pressure is 0 MPa, the speed of the roller leaving the hose increases with increasing rotation speed, and the backflow is more obvious, as shown in Figure 12a–c. When the rotation speed is 35 r/min, streamline diagrams of the roller in the hose at

different positions are shown. In the process of the roller gradually leaving from the lowest point, it can be seen from the three positions that the velocity streamline is evenly distributed. When the rotation speed is 50 r/min, the velocity streamline becomes slightly uneven. When the rotation speed is 65 r/min, At $t = t_0 + 280\Delta t$ moment, a clockwise vortex is formed, at $t = t_0 + 300\Delta t$ moment, a clockwise vortex disappears. As shown in Figure 13a–c, when the outlet pressure is 0.1 MPa, and the rotational speed is 35 r/min, the velocity streamline is almost the same as that without pressure. When the rotational speed is 50 r/min, at $t = t_0 + 390\Delta t$ moment, two clockwise rotating vortices of different sizes are formed, at $t = t_0 + 395\Delta t$ moment, one clockwise vortex disappears, at $t = t_0 + 400\Delta t$ moment, the other one disappears. When the rotational speed is 65 r/min, at $t = t_0 + 270\Delta t$ moment, a clockwise vortex is formed, the vortices are formed earlier and larger, forming a larger clockwise rotating stall chamber, at $t = t_0 + 270\Delta t$ moment, the roller just leaves the hose, a clockwise vortex does not disappear. It can be inferred that the corresponding vortex is caused by the countercurrent structure, and the pressure variation of the relative velocity pressure side and the suction side is quite different, which has a great influence on the pressure in the pipeline.

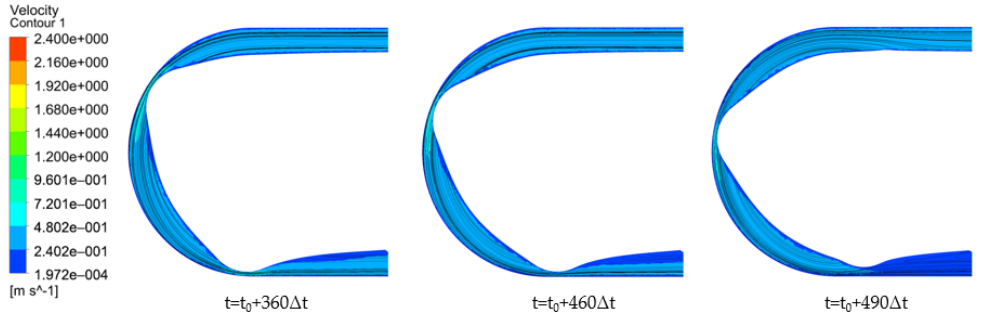

(**a**) 35 r/min

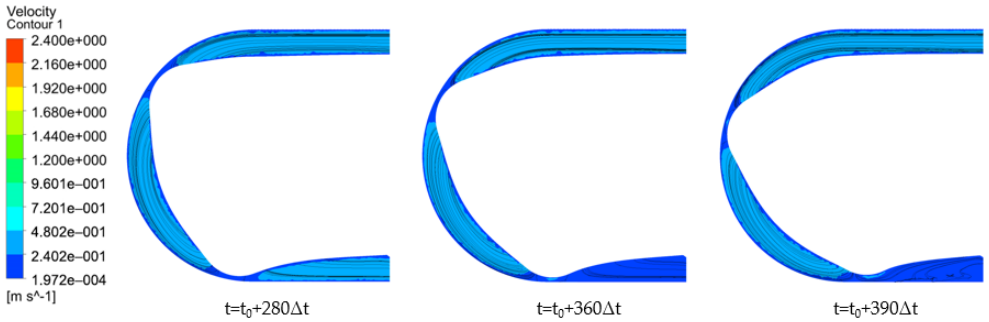

(**b**) 50 r/min

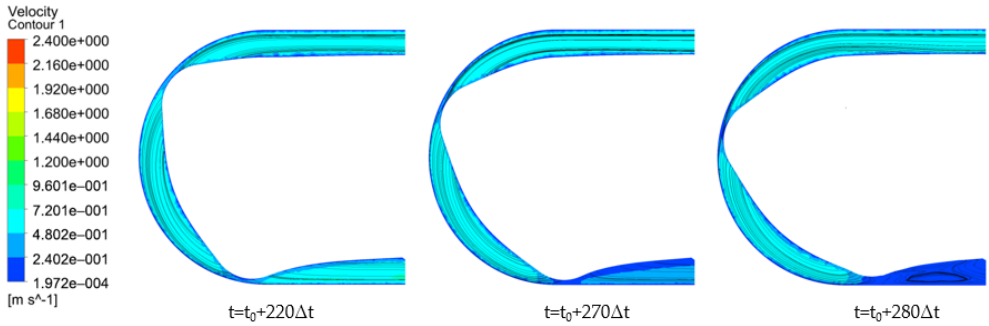

(**c**) 65 r/min

Figure 12. Flow line diagram of the 0 MPa outlet pressure at different speeds.

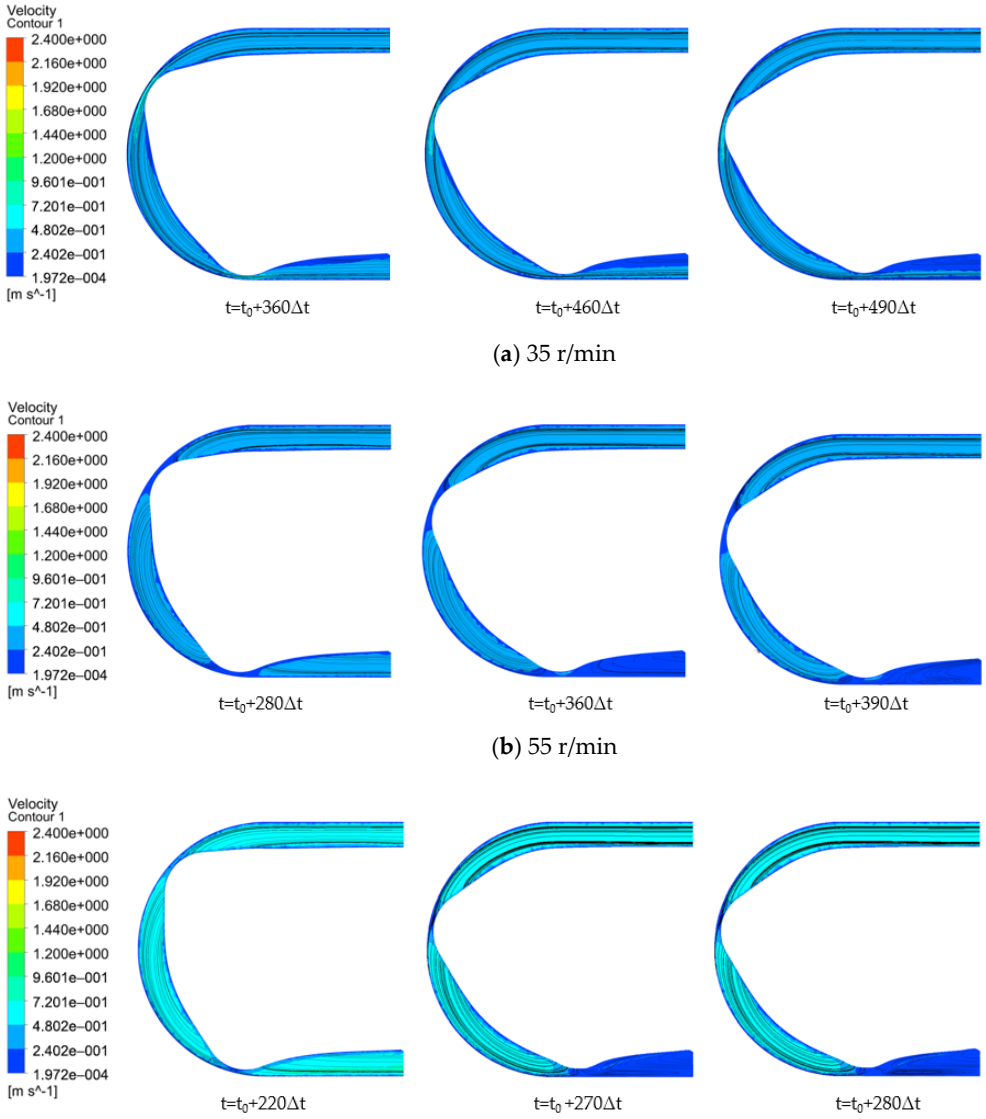

Figure 13. Flow line diagram at a 0.1 MPa outlet pressure at different speeds.

At the same speed, with increasing pressure, the vortex at the same position increases. When the roller leaves the rubber hose, the velocity streamline in the rubber hose shows circumferential non-uniformity. The maximum relative vorticity is around the cavity where the roller leaves the hose, and the vorticity gradually moves to the right. The strength of the vorticity is far away from the inner wall of the hose. There is obvious vorticity on the pressure surface, which indicates that there are vortices in the region. This phenomenon increases the unsteady flow in the pump, and the unsteady flow affects the pulsating pressure. Under the same pressure, with increasing rotating speed, the non-uniformity of the vorticity increases. As the pump speed increases and the outlet pressure increases, the non-uniformity becomes increasingly obvious. The fluid in the hose pump is divided into two parts along the channel. The roller leaves the hose, and the recovery deformation area of the hose is divided into two parts. In one part, the next roller rotates to make the fluid flow forward to fill the cavity, and in the other part, some backflow occurs due to the outlet pressure. Through numerical simulation analysis, the full three-dimensional unsteady flow field in the hose of the hose pump is obtained.

4.3. Time Domain Analysis of Pressure Fluctuation

Figures 14 and 15 show the experimental pressure pulsations at 35 r/min, 50 r/min, and 65 r/min when the outlet pressure is 0 MPa and 0.1 MPa, respectively. In the experimental results, three peaks and valleys are clearly depicted in all cases. Three peaks and valleys indicate that three rollers on the spindle pass through one revolution of the spindle.

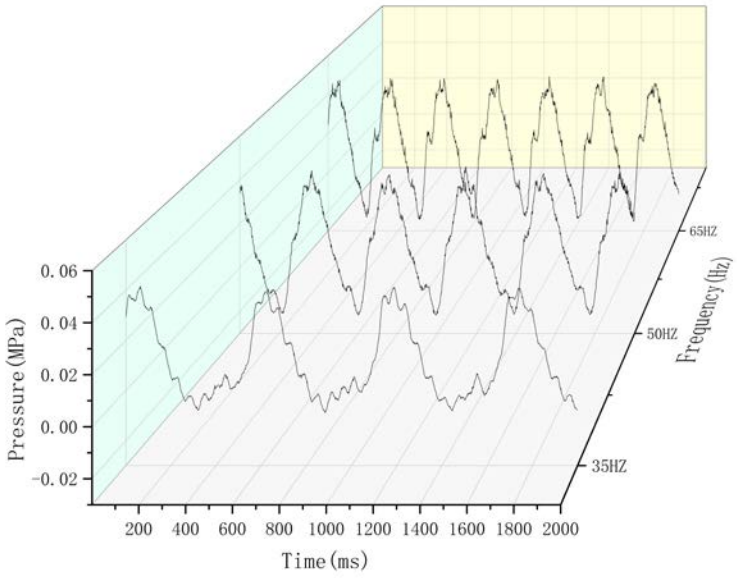

Figure 14. Pulsating pressure experimental results at different speeds with an outlet pressure of 0 MPa.

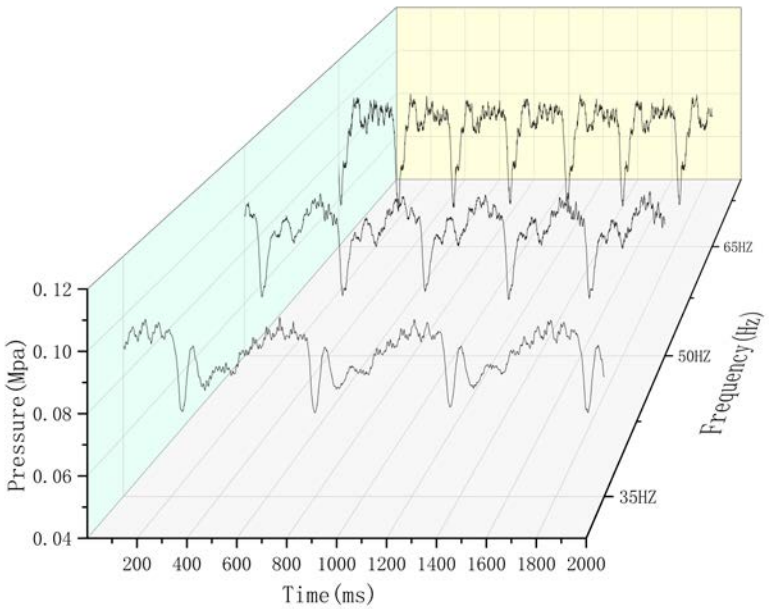

Figure 15. Pulsating pressure experimental results at different speeds with an outlet pressure of 0.1 MPa.

According to the experimental and simulated pulsating pressures, the pulsating pressure at the outlet decreases gradually when the pressure roller leaves the hose. When the pressure roller leaves the hose completely, the pressure reaches the minimum. Then, as the fluid is squeezed by the next roller and the return flow fills the deformation area of the hose, the fluid flows forward, and the pressure increases slowly. When the outlet pressure

is 0 MPa and the speed is 35 r/min, the experimental amplitude is (−0.01–0.04 MPa); when the speed is 50 r/min, the experimental amplitude is (−0.02–0.045 MPa); and when the speed is 65 r/min, the experimental amplitude is (−0.0–0.045 MPa). As shown in the figure, the pressure fluctuation curves of the three working conditions are similar, and the pressure change period is shorter when the rotating speed is higher. From the experimental data, it can be concluded that there is negative pressure in the pipeline, which is caused by the backflow of the pipeline. Under a high rotating speed, the backflow of the pipeline is faster, and the negative pressure is larger, which is the same as the above static pressure distribution.

When the outlet pressure is adjusted to 0.1 MPa and the rotation speed is 35 r/min, the experimental amplitude is (0.07–0.1 MPa); when the rotation speed is 50 r/min, the experimental amplitude is (0.06–0.1 MPa); and when the rotation speed is 65 r/min, the experimental amplitude is (0.03–0.1 MPa). It can be seen from the figure that when the outlet pressure is adjusted to 0.1 MPa, the pressure change of the pipeline is quite different from that when the outlet pressure is 0 MPa. Although the pressure of the whole pipe increases slowly when the pressure roller leaves the hose completely, there is a short rising state when the pressure roller leaves the hose gradually. This is due to the existence of outlet pressure, which forms a large stall area. This means that when the pressure and speed gradually increase, the pressure roller leaves the hose. The irregular flow pattern caused by the fluid stall in the hose has a great influence on the outlet pressure.

With increasing speed and outlet pressure, the amplitude of pressure pulsation gradually increases. Under partial load conditions, the internal flow characteristics and pressure pulsation show good consistency. The difference between the maximum and minimum values under partial load and overload operation conditions is greater in the mid plane. The curve shape at monitoring points 3 and 5 shows that the pressure fluctuation shows a downward trend under the same working conditions. At higher speed, the maximum deviation of the maximum pressure range is in the middle of the middle plane between the upper and lower inner walls of the hose, and the pressure decreases with the increase of the middle plane. Large deviations were also observed at higher speeds. Monitoring points 3 and 5 show the fluctuating behaviour of each roller leaving the hose under partial load and design load. The pressure pulsation under overload conditions is periodic in the inner wall of the cavity when the roller leaves the hose. The comparison between the internal flow characteristics and the pressure fluctuation shows good consistency under partial load conditions. Figures 16 and 17 clearly show that the amplitude of each monitoring point increases 1500 pa with increasing outlet pressure at the same speed and increases 1000 pa with increasing outlet pressure at the same speed. This shows that the irregular flow pattern caused by the rotating stall of the pressure roller has a great influence on the pressure in the inner cavity of the hose. In some cases, the effect of the rotating stall on the outlet pressure is also relatively large.

4.4. Pressure Pulsation at Monitoring Points

Due to the interaction between the rotating roller and the hose, the fluid in the hose shows unsteady flow characteristics. The monitoring points set around the area where the roller is about to leave compare the pressure fluctuation of a plane during the complete process of the roller leaving the hose gradually, as shown in Figure 16. According to the above discussion, compared with other working conditions, the pressure fluctuation in the hose is smaller when the speed is lower than that of the outlet pressure. The maximum pressure value is reached under partial load conditions. With increasing speed, the pulsation intensity increases. There are subtle differences between the maximum and minimum values at monitoring points 1 and 2. At the same time, the pulsating pressure in the hose changes periodically under conditions of no pressure. In addition, the pressure fluctuation in the hose is still irregular at high speed, and the range of pressure fluctuation increases by 3500 Pa. By observing the curve shape of each monitoring point, with the rotation of the roller, the gap between the upper and lower inner walls of the hose increases

gradually, and the pressure range decreases. The difference between the maximum and minimum values under partial load and overload operation conditions is greater in the mid plane. At the point far away from the outside circle of the press roll, the pressure value is usually lower. The curve shape at monitoring points 3 and 4 shows that the pressure fluctuation decreases under partial load and design operation conditions, reduced by about 500 pa. When the outlet pressure is 0.1 MPa, as shown in Figure 17, a large deviation is observed at a higher speed. Monitoring points 3 and 5 show the fluctuation behaviour of each roller under partial load conditions, and the pressure fluctuation is non-periodic behaviour in the hose. The comparison between the internal flow characteristics and the pressure fluctuation shows good consistency under partial load conditions. In Figure 17, it can be seen that the pressure amplitude clearly decreases 1500 pa from monitoring points 3 to 5. From the fluctuation pressure change diagram of monitoring point 7, the fluctuation pressure amplitude of three rotational speeds is relatively unchanged, and the differences between 35 r/min and 50 r/min and 65 r/min can be seen from the curve shape, which indicates that the irregular flow pattern caused by the rotating stall of the flow body in the hose has a certain influence on the pressure fluctuation in the hose.

4.5. Frequency Analysis

To obtain more inferences from the flow behaviour inside the pump, the study of pressure fluctuation is further explained in the frequency domain. Thus, it is possible to identify any irregular flow pattern during operation. Using the fast Fourier transform (FFT), the measured data from the pressure sensor on the outlet pipe and the simulation results from the monitoring points around the plane in each comparative load condition are used in the frequency domain. Figure 18a,b show the frequency domain experimental results under different operating conditions. The frequency domain range of each speed is between 0 and 500 Hz, plotted on the x-axis. The z-axis represents the dimensionless amplitude of the pressure. The shaft frequency FS appears at 5 Hz, which is the highest peak under the operation conditions. At the same time, in other operation conditions, when the speed is 65 r/min at 0.1 MPa, the record is the highest. The blade is excited by the frequency FB as a multiple of the shaft frequency, and the next highest peak is excited at 225 Hz, which implies that all operating conditions of noise and vibration are generated. As shown in Figures 19 and 20, in the frequency domain of the measured data, the amplitude of the roller passing through the frequency can be clearly seen. With increasing frequency, the amplitude decreases under all working conditions. When the outlet pressure is 0 MPa and 0.1 MPa, the lowest amplitude of FS appears at monitoring point 7 in Figures 19 and 20. When the outlet pressure is 0 MPa, the maximum amplitude of FS appears at monitoring point 3 in Figure 16. When the outlet pressure is 0.1 MPa, the maximum amplitude appears at monitoring point 1 in Figure 16. The pressure pulsation in these areas reaches the highest intensity under partial load conditions. The flow back in the hose has a great influence on the pressure fluctuation, and the amplitude at the passing frequency of each roller is larger. On the whole, the pressure fluctuation data measured by the experiment are in good agreement with the simulated pressure fluctuation data.

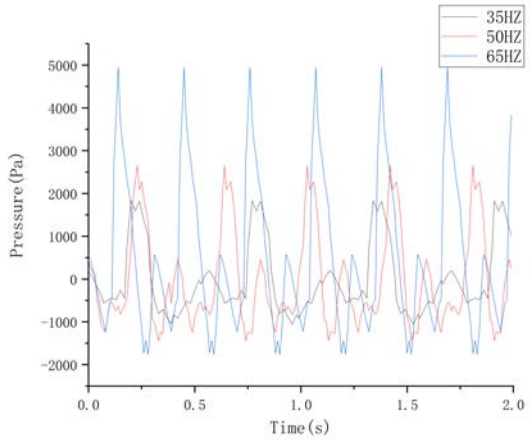

(**a**) Point 1

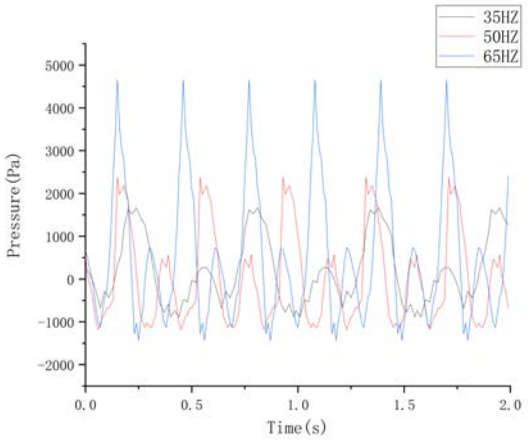

(**b**) Point 2

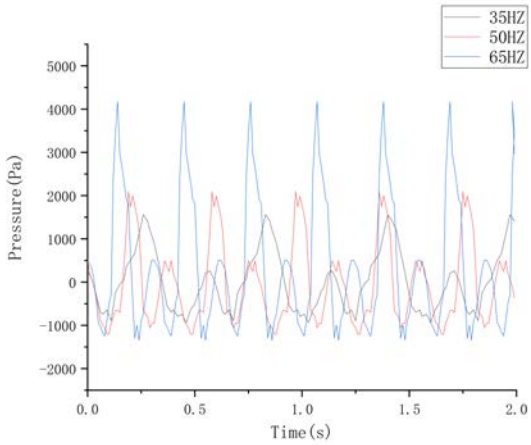

(**c**) Point 3

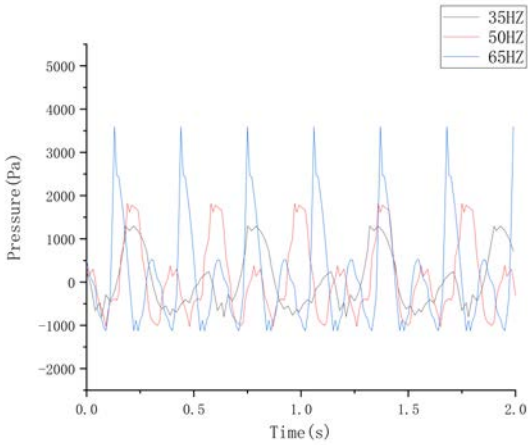

(**d**) Point 4

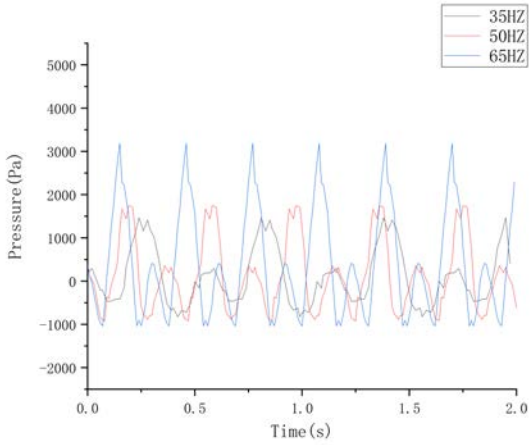

(**e**) Point 5

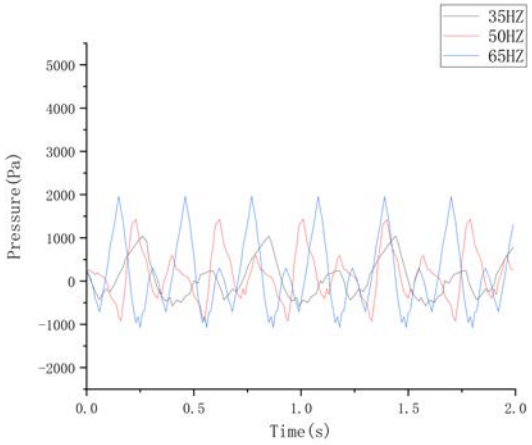

(**f**) Point 6

Figure 16. *Cont.*

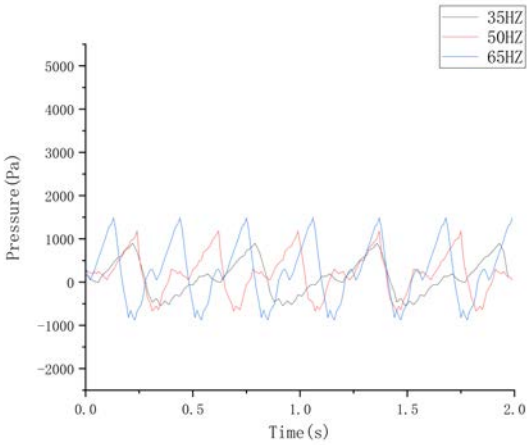

(**g**) Point 7

Figure 16. Pressure pulsation of the monitoring point under different speeds when the outlet pressure is 0 MPa.

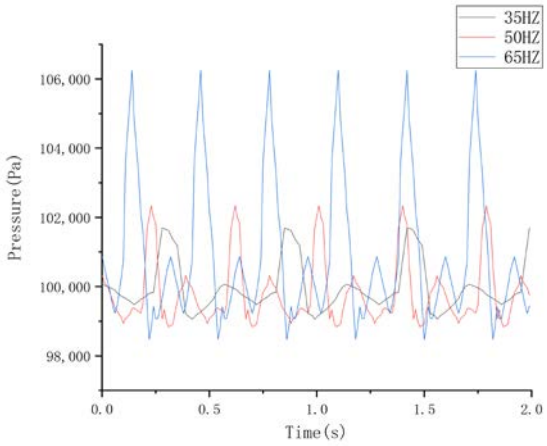

(**a**) Point 1

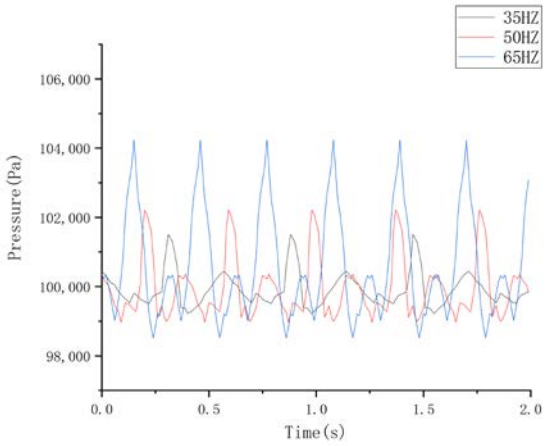

(**b**) Point 2

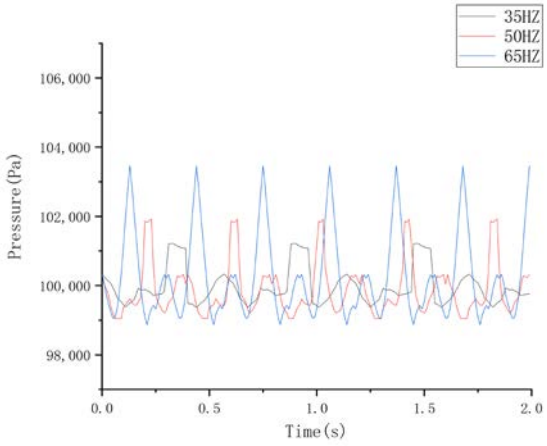

(**c**) Point 3

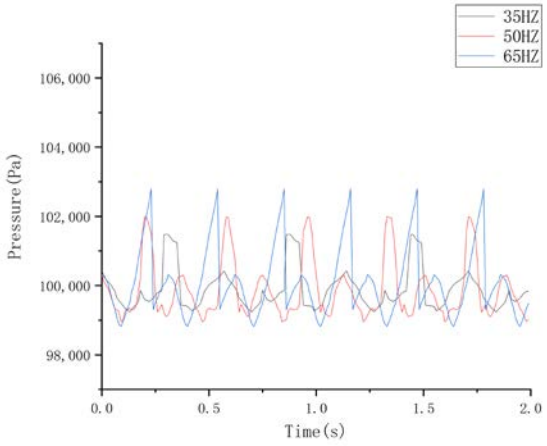

(**d**) Point 4

Figure 17. *Cont.*

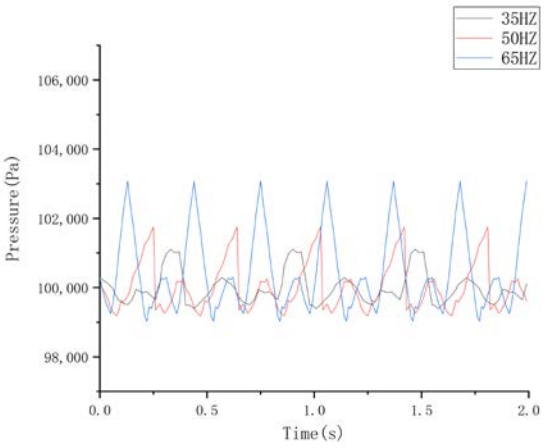

(**e**) Point 5

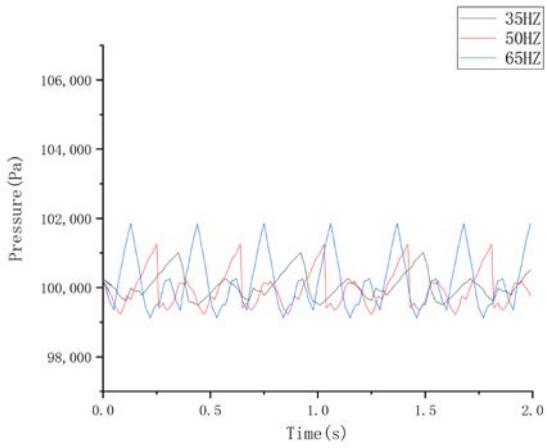

(**f**) Point 6

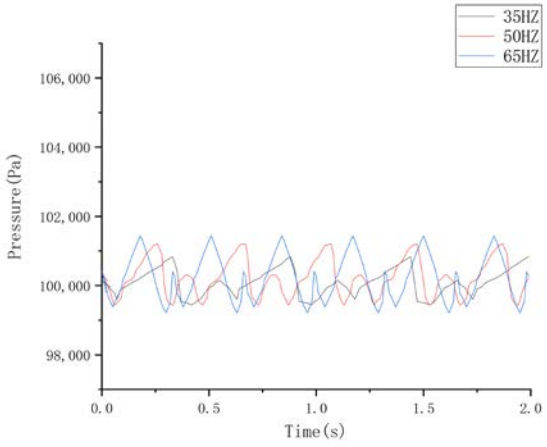

(**g**) Point 7

Figure 17. Pressure pulsation of the monitoring point under different speeds when the outlet pressure is 0.1 MPa.

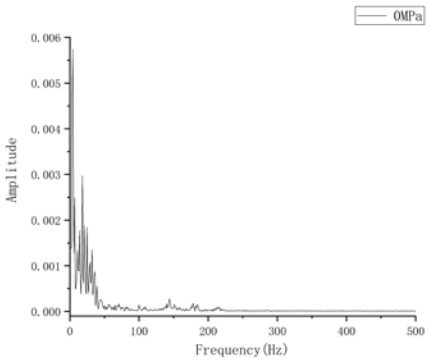

(**a**) Outlet pressure of 0 MPa

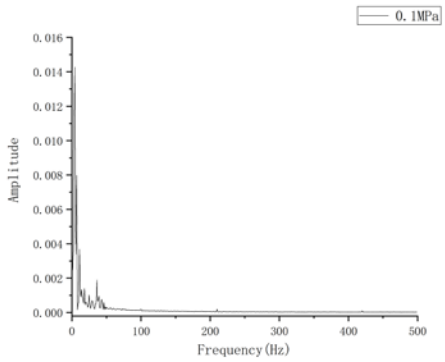

(**b**) Outlet pressure of 0.1 MPa

Figure 18. Experimental study on the pressure fluctuation in the pipeline in the frequency domain.

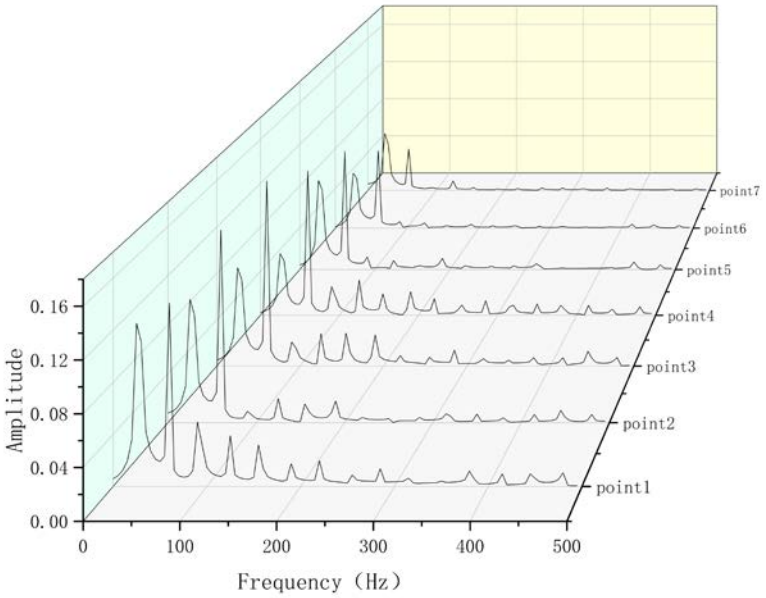

Figure 19. Pressure fluctuation in the area of hose recovery deformation calculated in the frequency domain when the outlet pressure is 0 MPa.

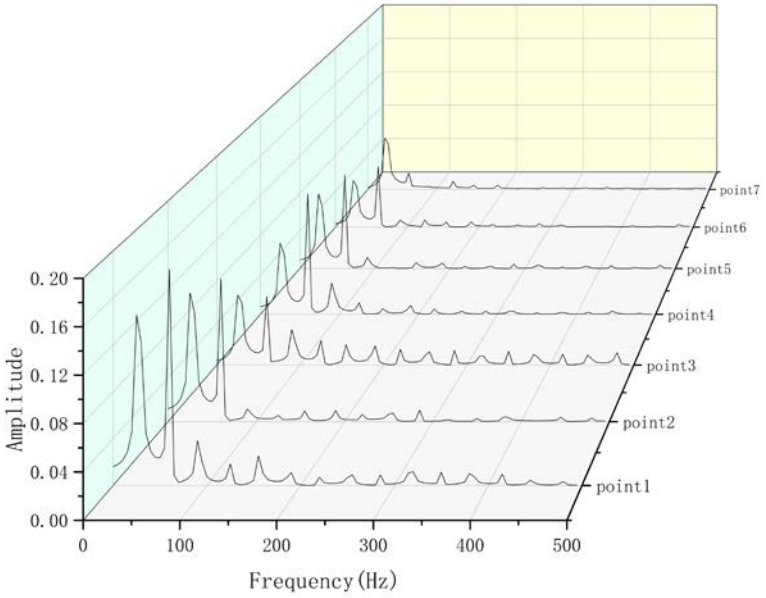

Figure 20. Pressure fluctuation in the area of hose recovery deformation calculated in the frequency domain when the outlet pressure is 0.1 MPa.

5. Conclusions

The pressure fluctuation characteristics in the whole flow channel of the hose pump under different working conditions were studied by numerical simulation and experiment. The following are some main findings and suggestions, which can be considered in the process of pump design optimization to improve the operational reliability of the pump.

1. The pressure pulsation of the hose pump is mainly caused by the large deformation of the hose when the hose is squeezed by the pressure roller. The smaller the middle plane of the inner wall of the hose deformation recovery area is, the larger the pressure fluctuation amplitude is, compared with the maximum middle plane, the difference is about 3000 pa. The main frequency of pressure fluctuation at different monitoring points where the roller leaves the hose is the passing frequency of the roller.

2. Under the same pressure, the amplitude of the main frequency at the outlet of the hose pump increases with increasing rotating speed. Under the same rotating speed, the amplitude of the main frequency at the outlet of the hose pump increases with increasing pressure. At the same speed, the main frequency amplitude of pressure fluctuation at the same monitoring point increases with increasing pressure, and at the same pressure, the main frequency amplitude of pressure fluctuation at the same monitoring point increases with increasing speed.

3. When the outlet pressure is 0 MPa, the fluid flows back along the whole fluid channel when the roller gradually leaves the hose. When the rotation speed increases, the speed of the roller leaving the hose increases, the speed of the fluid return increases, a small stall area forms in the lower-right part of the cavity, and the size of the stall area increases with increasing speed. When the outlet pressure is 0.1 MPa, which is slightly different from that without pressure, the fluid flows back along the inner wall of the hose and form a stall zone earlier 0.02 s than that without pressure. It does not disappear with the rotation of the roller.

4. With increasing rotational speed and pressure, the reverse flow structure of the hose recovery deformation area is obvious, and stall areas of different sizes form. Therefore, it is suggested to optimize the roller geometry, reduce the speed of the roller leaving the hose, and change the angle of the hose outlet.

Author Contributions: Conceptualization, W.W. and L.Z.; software, W.W.; validation, X.M., Z.H. and W.W.; resources, W.W.; data curation, Y.Y.; Writing—Original draft preparation, W.W.; writing—review and editing, W.W., L.Z.; project administration, L.Z.; funding acquisition, L.Z. All authors have read and agreed to the published version of the manuscript.

Funding: This research was funded by National Natural Science Foundation of China, grant number 52065055.

Institutional Review Board Statement: Not applicable.

Informed Consent Statement: Not applicable.

Data Availability Statement: All relevant data presented in the article are stored according to institutional requirements and, as such, are not available online. However, all data used in this Manuscript can be made available upon request to the authors.

Conflicts of Interest: The authors declare no conflict of interest.

References

1. Li, F.; Huang, W. Main use and design calculation of RGB hose pump. *Mechanics* **1998**, *25*, 29–30.
2. Yang, J. On the design of extrusion pump. construction machinery. **1998**.
3. Tao, J. Study on Characteristics of A High-flow Peristaltic Pump and Design of the Test System Huazhong University of Science and Technology. **2014**.
4. Wu, H. Research On Characteristics Of Micro-Peristaltic Pump Based On Stepper Motor Harbin Institute of Technology.
5. Takabatake, S.; Ayukawa, K.; Mori, A. Peristaltic pumping in circular cylindrical tubes: A numerical study of fluid transport and its efficiency. *J. Fluid Mech.* **1988**, *193*, 267–283. [CrossRef]
6. Takabatake, S.; Ayukawa, K. Numerical study of two-dimensional peristaltic flows. *J. Fluid Mech.* **1982**, *122*, 439. [CrossRef]
7. Sorensen, G.P.; Akkas, T. Peristaltic pump and cassette. U.S. Patent 6572349, 2001.
8. Liu, W.; Liu, X.; Chan, R. Research on peristaltic pump design based on patent analysis. *J. Eng. Des.* **2013**, *20*, 361–367.
9. Zhang, Y. *Research on Analysis and Optimistic Design of Industrial Hose Pump Using thorough Cycle Simulation and Meta-Model Method*; Zhejiang University: Hangzhou, China, 2017.
10. Lan, Z. Current situation and development of gear pump research. *Lift. Transp. Mach.* **2005**, *6*, 11–13.
11. Liu, X. Structure principle and application of peristaltic pump. *Fluid Mach.* **1998**, *12*, 38–40.
12. Li, D. Flexible hose pump and its application in phosphate fertilizer production. *Phosphate Compd. Fertil.* **2002**, *17*, 64–65.
13. Chen, Y.; Min, Q.; Zhang, X. Tubing Pump and Its Application to Fertilization of Liquid Fertilizers. *J. Agric. Mach.* **2005**, *36*, 54–56.
14. Shamanskiy, A.; Simeon, B. Mesh deformation techniques in fluid-structure interaction: Robustness, accumulated distortion and computational efficiency. *arXiv* **2020**, arXiv:2006.14051.
15. Yakhlef, O.; Murea, C.M. Numerical Simulation of Dynamic Fluid-Structure Interaction with Elastic Structure–Rigid Obstacle Contact. *Fluids* **2021**, *6*, 51. [CrossRef]

16. Akbay, M.; Schroeder, C.; Shinar, T. Boundary pressure projection for partitioned solution of fluid-structure interaction with incompressible Dirichlet fluid domains. *J. Comput. Phys.* **2020**, *425*.
17. Ning, J.; Zhang, H.; Xu, X.; Ma, T. A novel fluid-structure interaction algorithm for compressible flows and deformable structures. *J. Comput. Phys.* **2020**, *426*, 109921. [CrossRef]
18. Zhou, X.; Liang, X.M.; Zhao, G.; Su, Y.; Wang, Y. A new computational fluid dynamics method for in-depth investigation of flow dynamics in roller pump systems. *Artif. Organs* **2014**, *38*, E106–E117. [CrossRef]
19. Pdf, E. Fluid-Structure Interaction Analysis of a Peristaltic Pump. In Proceedings of the 2011 COMSOL, Boston, MA, USA, 25 February 2011.
20. Wang, D.; Chen, Z.; Han, Y.; Li, J. Theoretical Calculation and Experimental Investigation of Peristaltic Pump Flow. *Chem. Autom. Instrum.* **2015**, *2*, 186–187, 216.
21. Liu, J.; Li, J.; Shi, Y.; Zhu, X. Structure Optimization of Peristaltic Pump in Water Fertilizer Integrated Irrigation Device. *Water Sav. Irrig.* **2021**, *2*, 70–74.
22. Balabel, A.; Dinkler, D. Turbulence models for fluid-structure interaction applications. *Emir. J. Eng. Res* **2006**, *11*, 1–18.
23. Barbagallo, R.; Sequenzia, G.; Cammarata, A.; Oliveri, S.M.; Fatuzzo, G. Redesign and multibody simulation of a motorcycle rear suspension with eccentric mechanism. *Int. J. Interact. Des. Manuf.* **2017**. [CrossRef]
24. Simone, M.; Guida, D. Identification and control of a Unmanned Ground Vehicle by using Arduino. UPB Scientific Bulletin, Series D. *Mech. Eng.* **2018**, *80*, 141–154.
25. Cammarata, A. Optimized design of a large-workspace 2-DOF parallel robot for solar tracking systems. Mechanism and Machine Theory: Dynamics of Machine Systems Gears and Power Trandmissions Robots and Manipulator Systems Computer. *Aided Des. Methods* **2015**, *83*, 175–186.
26. Formato, G.; Romano, R.; Formato, A.; Sorvari, J.; Villecco, F. Fluid–Structure Interaction Modeling Applied to Peristaltic Pump Flow Simulations. *Machines* **2019**, *7*, 50. [CrossRef]
27. Chakraborty, D.; Prakash, J.R.; Friend, J.; Yeo, L. Fluid-Structure Interaction in Deformable Microchannels. Phys. *Fluids* **2012**, *24*, 3461–3473.
28. Yan, Q. Large deformation finite element analysis for rubber matrix composite structures. *J. Comput. Mech.* **2002**, *19*, 477–481.
29. Li, Z. Research and Design of BQ Peristaltic Pump Delivery System Huazhong University of Science and Technology. 2017.
30. Bergstrom, J.S. *Mechanics of Solid Polymers: Theory and Computational Modeling*, William Andrew. 2015.
31. Zhou, X. *Researeh of Hose Invalidation Factor and ImProvement of Hose PumP Structure*; Beijing Forestry University: Hangzhou, China.
32. Chen, Y. *Structure Analysis on Rubber Hose of Hose Pumps Based on Nonlinear Finite Element Method*; Beijing Forestry University: Hangzhou, China, 2006.